Climatology of medium-scale traveling ionospheric disturbances observed by a GPS network in central China

Feng Ding,[1] Weixing Wan,[1] Guirong Xu,[2] Tao Yu,[3] Guanglin Yang,[3] and Jing-song Wang[3]

Received 9 February 2011; revised 29 June 2011; accepted 7 July 2011; published 29 September 2011.

[1] The 15-month climatology of medium-scale traveling ionospheric disturbances (MSTIDs) during a solar minimum period has been constructed from observations of a dense GPS receiver array in Central China. In total, 793 MSTID events are identified, with peaks in occurrence at 1500 LT and 0100 LT. The occurrence of MSTIDs decreases following an increase in geomagnetic activity, with 46% of the MSTIDS occurring in the daytime. Daytime MSTIDs are characterized by a major occurrence maximum around the winter solstice and by an equatorward propagation direction. The period, phase velocity, azimuth, and amplitude of daytime MSTIDs are 20–60 min, 100–400 m/s, 130°–270°, and 0.8–1.5%, respectively. The remaining 54% of the MSTIDs occurred at night, and were characterized by a peak in occurrence at the summer solstice and by a southwestward propagation direction. The period, phase velocity, azimuth, and amplitude of nighttime MSTIDs are 20–70 min, 50–230 m/s, 170°–300°, and 2–7%, respectively. The propagation directions and the seasonal behaviors support the view that daytime MSTIDs are an ionospheric manifestation of atmospheric gravity waves from the lower atmosphere, while a possible excitation mechanism of nighttime MSTIDs is the electrodynamics process caused by plasma instability in the F layer.

Citation: Ding, F., W. Wan, G. Xu, T. Yu, G. Yang, and J. Wang (2011), Climatology of medium-scale traveling ionospheric disturbances observed by a GPS network in central China, *J. Geophys. Res.*, *116*, A09327, doi:10.1029/2011JA016545.

1. Introduction

[2] Medium-scale traveling ionospheric disturbances (MSTIDs) are wave-like perturbations of the ionospheric plasma with wavelengths of several hundred kilometers and velocities of several hundred meters per second. These are one of the most common ionospheric phenomena at mid and low latitudes. For many years, MSTIDs were observed by HF Doppler [*Georges*, 1968; *Waldock and Jones*, 1986; *Wan et al.*, 1998], ionosonde [*MacDougall and Hall*, 1998; *Ashkaliev et al.*, 2003], airglow imager [*Shiokawa et al.*, 2003], incoherent scatter radar [*Pinger*, 1979], and the total electron content technique [*Morton and Essex*, 1978]. Early on, MSTIDs were generally observed using local arrays or several stations that monitored the characteristics of MSTIDs in local regions. The development of satellite observations and dense distributions of stations in the late 1990s enabled scientists to observe the two-dimensional structure of MSTIDs over a much wider area and to investigate their excitation and propagation features at various latitudes and local times [*Saito et al.*, 1998; *Tsugawa et al.*, 2007].

[3] Previous studies proposed several candidates as the sources of MSTIDs. Some reported that MSTIDs observed at mid and high latitudes can be excited by auroral activity [*Richmond*, 1978; *Hunsucker*, 1982]; however, the main sources of MSTIDs appear to be tropospheric meteorological processes such as the jet stream [*Bertin et al.*, 1978; *Buss et al.*, 2004], thunderstorms [*Pierce and Coroniti*, 1966; *Baker and Davies*, 1969], hurricanes [*Tsutsui and Ogawa*, 1973; *Ibrahim et al.*, 2010], vortices [*Wan et al.*, 1998], and cold fronts [*Boška and Šauli*, 2001]. MSTIDs reported by these authors could be observed both in the daytime and at night. Atmospheric gravity waves are generated during meteorological processes, propagating obliquely upward in the ionosphere and manifesting themselves as traveling ionospheric disturbances. As the disturbances propagate for several hundred kilometers in the background wind field, they tend to propagate in the opposite direction to that of thermosphere winds as a result of wind-filtering effects [*Waldock and Jones*, 1984; *Ding et al.*, 2003]. Their preferred propagation direction varies depending on the location, wind, and the relative positions of the observation and source regions [*Cowling et al.*, 1971].

[1]Beijing National Observatory of Space Environment, Institute of Geology and Geophysics, Chinese Academy of Sciences, Beijing, China.
[2]Institute of Heavy Rain, China Meteorological Administration, Wuhan, China.
[3]National Center for Space Weather, China Meteorological Administration, Beijing, China.

0148-0227/11/2011JA016545

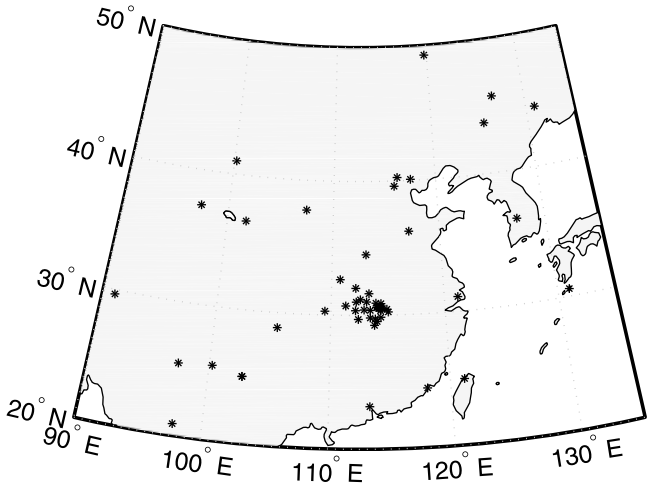

Figure 1. Locations of GPS stations around China.

[4] Another possible source of MSTIDs is electrodynamic instability in the F layer, as proposed by *Perkins* [1973] and *Kelley and Miller* [1997]. Since the 1990s, with the development of networks of GPS receivers and arrays of all-sky airglow imagers, many nighttime MSTIDs have been observed in various regions, including Puerto Rico [*Beach et al.*, 1997; *Garcia et al.*, 2000; *Martinis et al.*, 2010], USA [*Tsugawa et al.*, 2007; *Kotake et al.*, 2007], Japan [*Shiokawa et al.*, 2003], Taiwan [*Lee et al.*, 2008], and South America [*Candido et al.*, 2008]. These MSTIDs always propagate southwestward in the Northern Hemisphere and northwestward in the Southern Hemisphere. Further studies indicated that nighttime MSTIDs are likely to be related to the active development of plasma instabilities in the ionospheric F layer [*Kelley and Miller*, 1997]. The instability, which is strong in the night side, can generate local polarization electric fields that move the plasma by $\mathbf{E} \times \mathbf{B}$ drift, causing perturbations in plasma density. The excitation mechanism of this type of MSTIDs is the subject of ongoing research [*Zhou and Mathews*, 2006; *Yokoyama et al.*, 2008].

[5] There are limited statistical studies of MSTIDs in the region of China. *Wan et al.* [1998, 2000] used a 6-year period (1985–1990) data observed by an HF Doppler array at Central China to study the seasonal change of MSTIDs. He found that MSTIDs in this area mainly propagate northeastward and southwestward. Through a reverse ray tracing method, *Wan et al.* [1998] showed that the source regions is located in the southeastern and northeastern edges of Qinghai-Tibet plateau, where the tropospheric vortexes are frequently produced. *Xiao et al.* [2007] used HF Doppler shift data to monitor MSTIDs in North China during the periods of 24 strong typhoons from 1987 to 1992 and found that the excitation of MSTIDs is very effective when a typhoon is landing on or near a mainland coast. It is pointed out by *Xiao et al.* [2007] that, during the landing of a typhoon, the rapid loss of momentum due to viscous interaction could be an additional factor in exciting AGWs. However, these studies didn't include the data observed by GPS network in China.

[6] In this paper, we present the 15-month climatology of MSTIDs observed by a dense GPS receiver array located in Central China. The seasonal dependence and regional properties of nighttime and daytime MSTIDs are discussed based on the observation data.

2. Observations and Methods

[7] Total electronic content (TEC) data measured by a Global Positioning System (GPS) were obtained from 50 GPS stations (Figure 1) located throughout and around China: 26 stations of the Crustal Movement Observation Network of China and the International GNSS service (IGS), and 24 stations established by the Wuhan Institute of Heavy Rain, China Meteorological Administration. The latter 24 stations cover Hubei province in south Central China (29°N–33°N, 108°E–116°E) over an area of 190,000 km^2 at the northern boundary of the anomaly crest region. The observations cover a much wider area of seven provinces in Central China. The average distance between stations in Hubei province is ~50 km. We used data observed between January 2009 and March 2010.

[8] Figure 2 shows a two-dimensional TEC perturbation map for a case of MSTID observed by the GPS network on 29 July 2009. The deviation of TEC (DTEC) for each satellite–receiver pair is calculated by subtracting the 1-h running average from each TEC time series. We divided the area of 26°N–35°N, 106°E–118°E into pixels of size 0.5° × 0.5°. The TEC perturbation value for each pixel during a specific time interval is the average of DTEC from the observation of all GPS receiver–satellite pairs whose ionospheric pierce points pass over the pixel during the interval of interest. Figure 2 shows an MSTID propagating southwestward with a maximum amplitude of 0.4 TECU. The phase front, with a width of 300–900 km, moves southwestward over a distance of ~450 km.

[9] Because the GPS array in Hubei province was only recently established, observed/collected data may be discontinuous on certain days for some stations. This complicates any statistical analysis of the characteristics of MSTIDs based on DTEC maps. As an alternative, we use the multichannel maximum entropy method (MMEM) to analyze the data observed from several GPS stations (spaced at intervals of 20–40 km) and obtain the propagation parameters in the case of MSTIDs.

[10] Here, we introduce the method of MMEM in obtaining the propagation parameters of MSTIDs. First, we chose the TEC data from 3 GPS stations around Wuhan (30°N, 114°E) for our cross-spectral analysis. Data from these stations were chosen because they are available in most of the time, and a distance of ~20–40 km among them is suitable for analyzing the phase difference of MSTIDs observed in the TEC series by different stations.

[11] It is generally possible to simultaneously observe 2–8 slant TEC time series from a single station, with their line of sight (LOS) moving in different directions. Usually when a TID passes by, we can observe the TEC perturbation in more than one slant TEC series with different perturbation amplitudes. It was pointed out by *Jacobson et al.* [1995] that TEC signatures of TIDs are sensitive to the orientation of the line of sight. For each station, we selected one TEC time series with the maximum perturbation amplitude for the subsequent data processing. This ensures us to find the most significant signature of TIDs, though we didn't use the

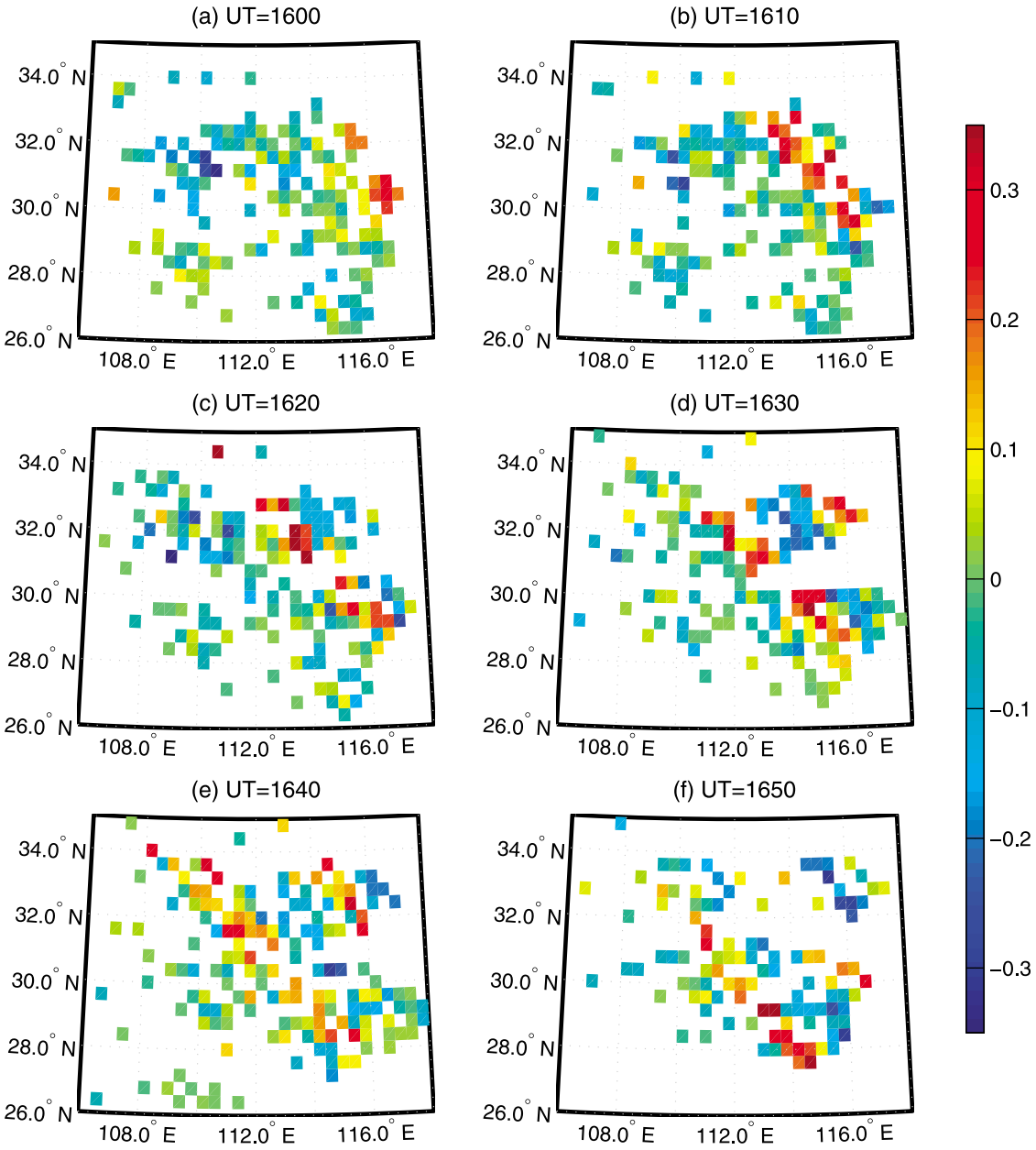

Figure 2. Two-dimensional maps of the derivation of TEC between 1600 UT and 1650 UT on 29 July 2009 in Central China.

information of perturbation from other observed series. We then got 3 slant TEC time series, corresponding to 3 stations.

[12] Next, we applied a running window of 1.2 h to each of the original TEC time series at intervals of 2 min, producing a sequence series with duration of 1.2 h. We then removed the background trends from these 1.2-h time series using residues obtained from polynomial fits. After that, we applied the multichannel maximum entropy method to each 1.2-h time series to yield the main frequency and phase differences among TEC perturbation series observed by different stations.

[13] It is necessary to consider the movement of the GPS satellites in our analysis, as this causes the movement of ionospheric pierce points and leads to the mixture of TEC variation both with space and time. *Wan et al.* [1997] found that the movement of ionospheric pierce points results in the offset of TIDs' frequency observed in TEC series, which is like the Doppler shift caused by the motion of the observation point. Under estimation, we found there is an offset of up to 30% in the main frequency of TIDs. We applied a Galileo transformation to adjust the TIDs' frequency through equation $\omega = \omega' + \mathbf{k} \cdot \mathbf{v}$, where ω and ω' are, respectively, the main frequency of TIDs observed in the Earth-fixed system and that observed in the coordinate system moving with the ionospheric pierce point, $\mathbf{k}$ is the horizontal wave vector, and $\mathbf{v}$ is an average of the moving velocity of the ionospheric pierce point during 1.2 h. A detailed development of such equation is described by *Wan et al.* [1997].

[14] Finally, based on the main frequency and phase differences thus obtained, we calculated the wave period,

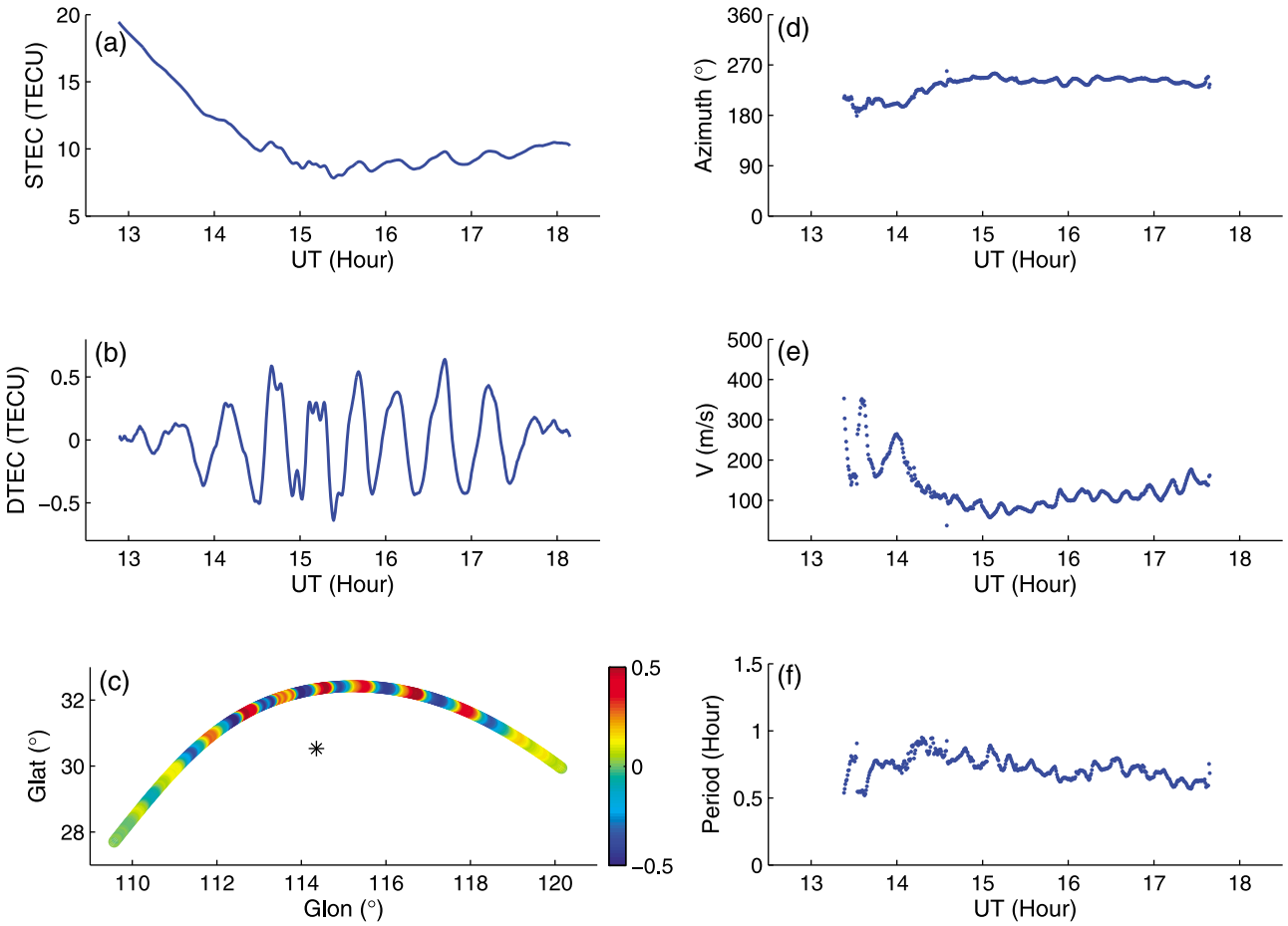

Figure 3. Temporal variations in (a) the slant TEC, (b) the derivation of TEC, (d) azimuth, (e) horizontal phase velocity, and (f) period. (c) The derivation of TEC along the path of an ionospheric pierce point in the longitude–latitude plane (unit of contours: TECU).The asterisk marks the location of the GPS station at Wuhan (30°N, 114°E), where the TEC was observed.

azimuth, and phase velocity through equations (4)–(7) of *Wang et al.* [2007]. Since each 1.2-h time series was separated by two minutes, the temporal variation of wave parameters across the observation time was revealed. In the case of a steady traveling ionospheric disturbance field passing by, the TID parameters would remain steady for the duration of the field.

[15] Three criteria are required during the identification of a MSTID event. First, wave-like variation in TEC series should last at least two cycles. Second, the maximum amplitudes of disturbances should exceed 0.5%. Last, the temporal variation of wave period, azimuth, and phase velocity obtained from MMEN method should not change too much. The last criterion is set to ensure that we observed a steady wavefield and that the parameters thus obtained are reliable.

[16] Figure 3 shows the results for an MSTID that occurred on 29 July 2009, including temporal variations in the slant TEC (Figure 3a) from GPS satellite PRN 4, the derivation of TEC (Figure 3b), azimuth (Figure 3d), horizontal phase velocity (Figure 3e), and period (Figure 3f). Figure 3c shows the derivation of TEC along the path of an ionospheric pierce point in the longitude–latitude plane (unit of contours: TECU). An MSTID event occurred between 1320 UT and 1740 UT (i.e., between 2120 LT and 0140 LT) with a maximum amplitude of 0.6 TECU (Figures 3a and 3b). The disturbances was observed in the range of 30.5°N–32.5°N, 112°E–119°E (Figure 3c). The period, velocity, and azimuth obtained from MMEM method remained largely unchanged during 1430–1740 UT (Figures 3d–3f). The MSTID propagated southwestward during this period with an average period, velocity, and azimuth of 42 min, 103 m/s, and 242°, respectively.

[17] It is generally possible to simultaneously observe 2–8 slant TEC time series from a single station, with their LOS moving in different directions. We chose the time series with the maximum perturbation amplitude for data processing. Using the MMEM method introduced above, we analyzed the TEC database between 1 January 2009 and 31 March 2010. The statistical results are presented in the next section.

3. Results

[18] We identified 793 MSTID events over the 453 observational days. The duration of MSTIDs varied from 1 to 6 h,

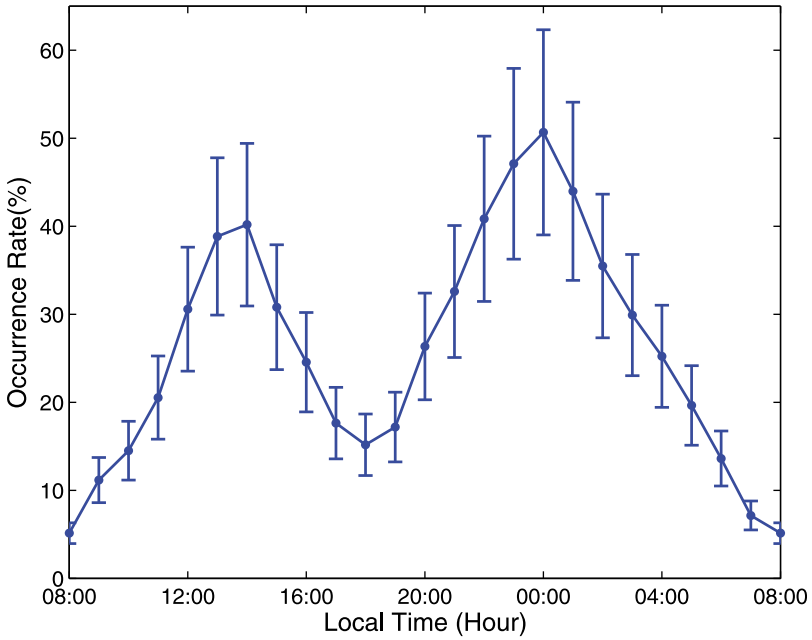

Figure 4. Local time dependence of the occurrence of MSTIDs observed by a GPS network in Central China between January 2009 and March 2010.The occurrence rate is defined as the ratio of the sum of the duration of TIDs to the total observation time. Error bars are shown, which represent the standard deviation of hourly occurrence rate.

and 46% of the MSTIDs occurred in the daytime with an average duration of 2.1 h. The period, phase velocity, and azimuth of daytime MSTIDs were 20–60 min, 100–400 m/s, and 130°–270° respectively, with value averages of 34 ± 11 min, 210 ± 70 m/s, and 210° ± 86°. The other 54% of the events occurred at night, with an average duration of 2.9 h. The period, phase velocity, and azimuth of nighttime MSTIDs were 20–70 min, 50–230 m/s, and 170°–300° respectively, with average values of 43 ± 10 min, 133 ± 52 m/s, and 240° ± 49°.

[19] Figure 4 shows the occurrence of MSTIDs as a function of local time. Herein, the occurrence is defined as the ratio of the sum of MSTID durations to the sum of the observation time within each specific LT hour. The occurrence data show a strong dependence on local time, with a major peak (~50%) around 0100 LT and a minor peak (~40%) around 1500 LT. The occurrence is minimized at dawn and dusk. Considering these findings, we separately analyzed the statistical results of daytime and nighttime MSTIDs.

[20] Figure 5 shows the seasonal dependence of the occurrence of daytime MSTIDs (red bars) and nighttime MSTIDs (blue bars). The definition of occurrence here is similar to that in Figure 4 but for each month. The occurrence varies between 10% and 26% for daytime MSTIDs, with the maximum around January and the minimum around April and September. MSTIDs occur much more frequently at night than during daytime. Nighttime MSTIDs are observed most frequently in June (occurrence rate of 53%); they are seldom observed in March.

[21] Figure 6 shows the seasonal dependence of the relative amplitudes of TIDs observed in daytime (Figure 6a) and nighttime (Figure 6b) between January 2009 and March 2010. The amplitude, which is the maximum of amplitude for every TID case, is shown by circles. The red curves show seasonal variations in the monthly median amplitude. The median amplitude of daytime MSTIDs ranges between 0.8% and 1.5%, while that of nighttime MSTIDs is between 2% and 7%. The median amplitude of daytime MSTIDs reaches a peak in January, while that of nighttime MSTIDs reaches a peak in June.

[22] Figure 7 shows the seasonal behavior of the propagation azimuth for daytime (Figures 7a–7c) and nighttime (Figures 7d–7f) MSTIDs. Polar plots are shown of the sum of the duration of TIDs (unit: hours) as a function of azimuth in winter (December–January), summer (May–August), and the equinoxes (March, April, September, and October). To show the seasonal change in azimuth for a whole year, only data for 2009 are shown. There is an obvious southwestward propagation preference for both daytime and nighttime MSTIDs in all the three seasons. Only daytime MSTIDs occurred in winter is an exception, which show some preference of propagating southward (~20% out of all winter daytime cases), southeastward (~30%) and southwestward (~50%), respectively. The total duration of nighttime MSTIDs shows a peak in summer with the azimuth 240°, while the duration of day-time MSTIDs show a peak in winter with the azimuth between 130° and 270°.

[23] Figure 8 shows the variability in the sum of the duration of MSTIDs (Figure 8a) and their occurrence (Figure 8b) as a function of the Kp index. For each case we chose the maximum Kp as the representative of Kp index during the time when the disturbance occurred. We then obtained the sum of duration corresponding to every specific value of the Kp index. The occurrence is calculated as the ratio of the sum of TIDs' duration corresponding to every

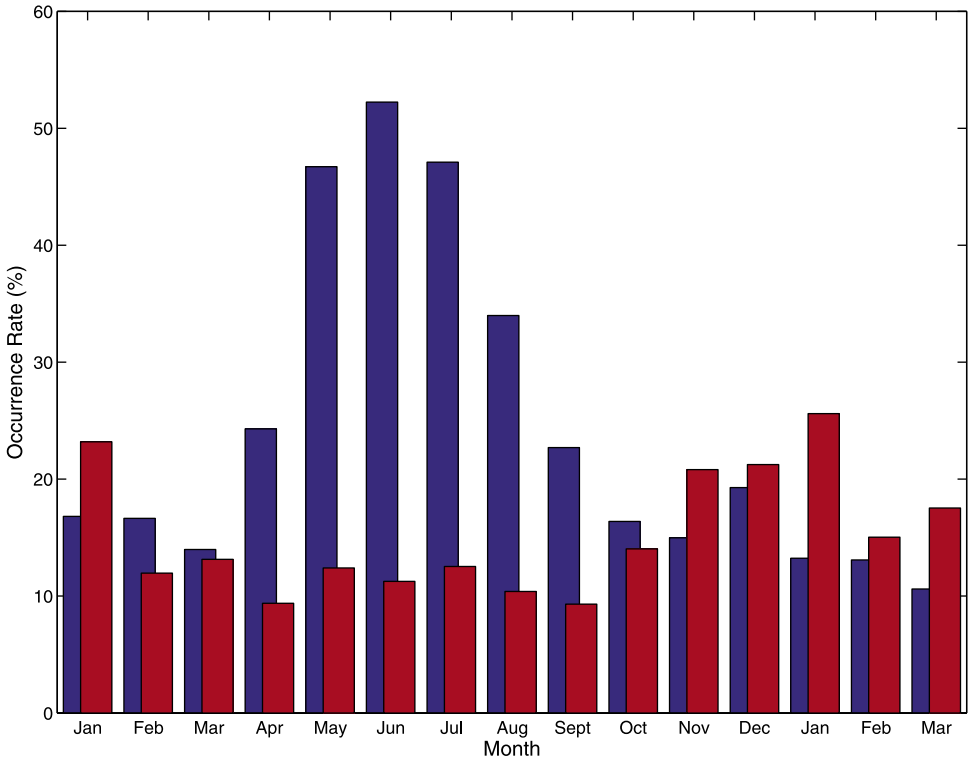

Figure 5. Seasonal dependence of the occurrence of daytime MSTIDs (red bars) and nighttime MSTIDs (blue bars).

specific Kp to the observational time. Because we observed MSTIDs during a solar minimum period, the maximum value of the Kp index was less than 3 on 90% of the observation days. There was no observation day with a maximum value of Kp index greater than 6-, and there were only 47 of 453 days with a maximum Kp index of between 3 and 6-. Eighty-eight percent of daytime MSTIDs and 91% of nighttime MSTIDs occurred on magnetically quiet days or on days with moderate disturbances, with Kp index values of less than 3 (Figure 8a). The duration and the occurrence show a trend of decreasing with increasing value of Kp index up until a value of 3 for both day-time and nighttime MSTIDs. These results indicate that MSTIDs tend occur more frequently and last longer during low magnetic activity period. We observed an increase in the occurrence of MSTIDs with increasing value of the Kp index between 3 and 4 (Figure 8b); however, given the small number of observation days with a Kp index greater than 3, this trend may not be representative.

[24] The inverse relation between solar activities and midlatitude MSTID occurrence was noted by some recent works. Using airglow observations, *Shiokawa et al.* [2003] reported an inverse dependence of MSTIDs with solar activity over Japan. Similarly, *Candido et al.* [2011] analyzed the yearly variation of the frequency spread F activities which were closely related to wave like-structures and found a decrease of the occurrence with the increase of Kp index. *Seker et al.* [2011] extensively investigated the relation between multiple magnetospheric state parameters and the occurrence of nighttime midlatitude plumes and MSTIDs. He pointed that MSTIDs tend to occur when the levels of Kp, Dst and AE were low and during interplanetary magnetic field north and interplanetary electric field west. These results imply a possible relation between the MSTIDs events and the condition of the magnetosphere and solar wind, even if F region irregularities are seeded at lower altitudes [*Seker et al.*, 2011].

4. Comparison and Discussion

[25] Figures 5–8 indicate that while there is little difference between daytime and nighttime MSTIDs in terms of their propagation azimuth and Kp dependence, there is significant difference regarding seasonal variations of occurrence and amplitude. In this section, we compare the present results with those of previous studies. The statistical features of daytime and nighttime MSTIDs are discussed in sections 4.1 and 4.2, respectively.

4.1. Daytime MSTIDs

[26] The results shown in Figures 5–7 indicate some common features of daytime MSTIDs observed by GPS TEC. They often have small amplitudes compared with nighttime MSTIDs (monthly mean amplitudes of up to 1.5%); their occurrence shows a peak in January, around the winter solstice; and they mostly propagate southward [*Evans et al.*, 1983], southeastward [*Kotake et al.*, 2007] or southwestward [*Tsugawa et al.*, 2007].

[27] The small amplitude of daytime MSTIDs is attributed to increased dissipation due to enhanced ion drag in the daytime [*Hocke and Schlegel*, 1996]. An occurrence maximum in winter and a southward preference for the direction of daytime MSTIDs have been observed previously by GPS networks in Japan [*Kotake et al.*, 2007] and in the USA

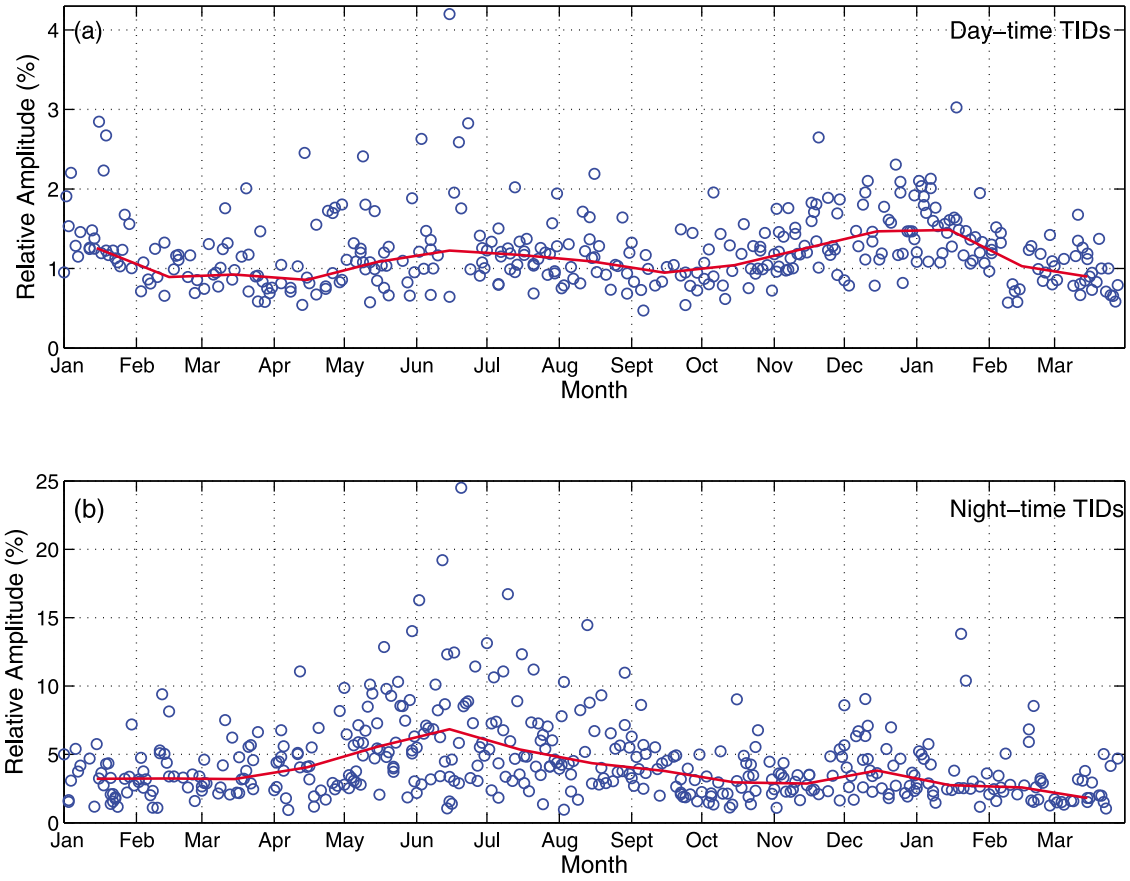

Figure 6. Seasonal dependence of the median amplitudes of TIDs observed in (a) daytime and (b) nighttime between January 2009 and March 2010. The median amplitude for each month is shown in circles for every TID case. The red curves show seasonal variations in the monthly median amplitude.

[*Tsugawa et al.*, 2007; *Kotake et al.*, 2006]. The features of daytime MSTIDs have also been reported in earlier studies. For example, based on Faraday rotation observations of VHF radars in Australia (37°S, 144°E), *Morton and Essex* [1978] found northeastward propagating MSTIDs, most of which were observed in the daytime. Using differential-Doppler measurements from five satellites of the Navy Navigation Series, *Evans et al.* [1983] observed MSTIDs propagating southward at Millstone Hill (43°N, 289°W), whose incidence seemed to increase in winter and at the equinoxes, and decrease in summer. *Waldock and Jones* [1986] observed many southeastward-propagating daytime MSTIDs during 1972–1975 by an HF Doppler array in Leicester, UK (52°N, 1°W). Using a satellite-beacon radio interferometer at New Mexico, USA (36°N, 106°E), *Jacobson et al.* [1995] found a peak in the occurrence of southward-propagating MSTIDs between midday and early afternoon at the winter solstice. Finally, based on the observations of an HF Doppler array in Central China during 1985–1990, *Wan et al.* [1998] detected the peak activity of MSTIDs in winter, with propagation mainly to the southeast and southwest. These previous observations indicate a peak in the occurrence of daytime MSTIDs around the winter solstice, regardless of location, and that daytime MSTIDs observed in midlatitude regions tend to propagate toward the equator.

[28] The observation methods used in the above studies are sensitive to MSTIDs at different observational heights. The reflection height of the HF signal is focused at 200–220 km, according to the HF Doppler observations undertaken by *Wan et al.* [1998]. GPS TEC data include variations in the ionosphere at all heights, and are mostly sensitive to ionospheric disturbances at around the height of the ionospheric pierce point (i.e., 300–400 km at midlatitudes). The consistent propagation features of daytime MSTIDs observed by various measurement techniques implies a close relation among MSTIDs observed at different heights. This finding supports the conventional theory that MSTIDs are ionospheric manifestations of atmospheric gravity waves (AGWs) propagating obliquely upward from the lower atmosphere [*Hines*, 1960]. Meteorological processes are a likely source of these MSTIDs [*Hocke and Schlegel*, 1996].

[29] The dominantly equatorward propagation of daytime MSTIDs probably reflects the directional filtering of background winds. Taking into account the effect of wind filtering on TIDs, AGWs propagating against the wind can easily reach the height of the ionosphere with relatively little energy attenuation compared with those propagating in the same direction as the wind [*Waldock and Jones*, 1984; *Ding et al.*, 2003]. This is consistent with the present observations, because the thermospheric wind blows poleward in

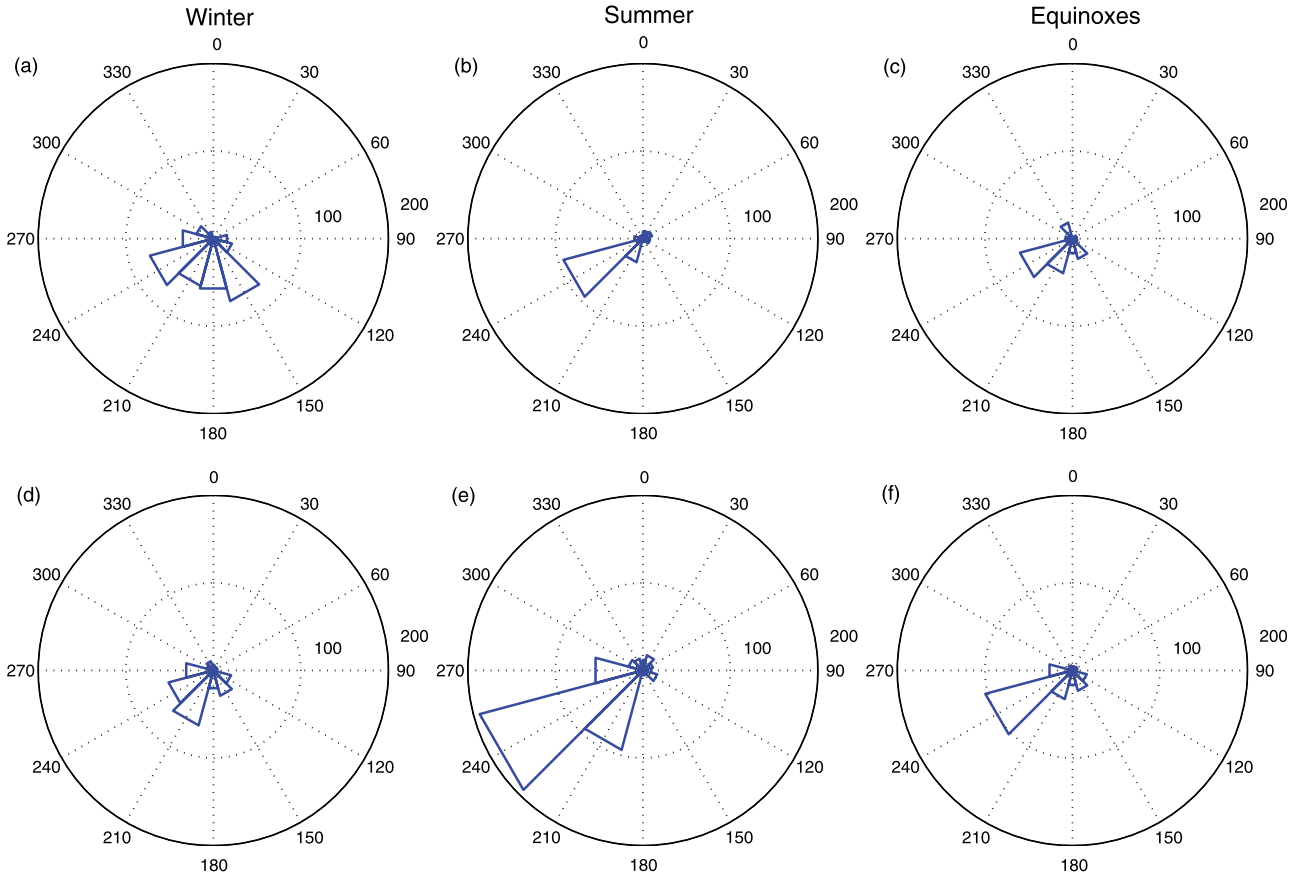

Figure 7. Seasonal behavior of the propagation azimuth for (a–c) daytime and (d–f) nighttime MSTIDs. Polar plots are shown of the sum of the duration of TIDs (unit: hours) as a function of azimuth in winter (December–January), summer (May–August), and the equinoxes (March–April and September–October). Only the data for 2009 are shown.

the daytime, and daytime MSTIDs propagate equatorward. The directional preference of daytime MSTIDs is also supported by the results of *Kelley and Miller* [1997], who showed that equatorward-propagating daytime gravity waves experience the least amount of ion drag, making them the most prominent in ionospheric observations.

[30] The occurrence peak of daytime MSTIDs around the winter solstice may be closely related to the filtering of AGWs by the steep temperature gradients in the atmospheric temperature profile within the mesopause region [*Kotake et al.*, 2006]. The steep gradient acts as an upper boundary for gravity waves, as upgoing waves with a short period are easily reflected at the gradient. Lidar observations at the Delaware Observatory, USA (32°N, 70°W), indicate that the temperature gradient is less steep in winter than in summer [*She and Lowe*, 1998]. Consequently, more

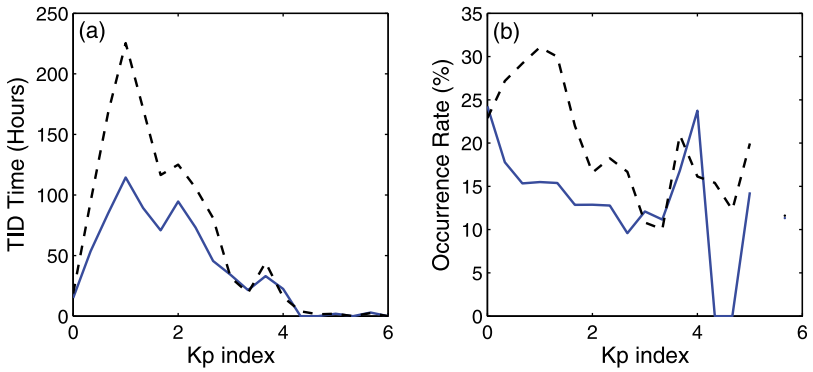

Figure 8. Variability in (a) the total duration of MSTIDs and (b) their occurrence rate as a function of the Kp index. The blue solid curves and black dashed curves indicate data for daytime and nighttime MSTIDs, respectively.

upgoing gravity waves are able to penetrate the ionosphere and cause MSTIDs in winter [*Bristow and Greenwald*, 1996].

[31] An earlier observation of MSTIDs using an HP Doppler array was conducted during 1985–1990 in a similar part of Central China to that considered in the present study [*Wan et al.*, 1998, 2000]. Three HF Doppler radars (separated by distances of ~100 km) were set in Hubei province to receive the timing signal broadcasted from Shanxi Observatory (35°N, 110°E). The observation was mostly effective in the daytime, with the reflection height of HF signals centered at 200–220 km. The HF Doppler observations revealed a major peak in the occurrence of MSTIDs during winter and a minor peak during summer. 42% of the MSTIDs tended to propagate southeastward, and 35% propagated northeastward. Other 12% propagated in the southwestward direction [*Wan et al.*, 1998]. The northeastward propagation is not seen in the present results based on GPS TEC data. This discrepancy may be due to contrasting observation heights among the different studies. The wind-filtering effect on upgoing AGWs is more intensive for disturbances at greater heights than for those at lower heights. Because the observational height of GPS TEC for TIDs is higher than that of HF Doppler, northeastward-propagating MSTIDs observed by HF Doppler may be filtered out at greater heights because of the poleward-blowing background wind in the daytime.

[32] The decrease in MSTIDs occurrence following an increase in geomagnetic activity, as observed in the present study, has been reported previously in many studies at mid and low latitudes [*Georges*, 1968; *Morton and Essex*, 1978; *Evans et al.*, 1983; *Hocke and Schlegel*, 1996; *Afraimovich et al.*, 2001; *He and Ping*, 2008]. However, some observations have been reported at mid and high latitudes, which show that in some cases, MSTIDs could still be observed during geomagnetic disturbances [*Richmond*, 1978; *Hunsucker*, 1982; *Bristow and Greenwald*, 1996]. In the present study, few MSTIDs occurred with a Kp index greater than 3 (Figure 8). But a statistical study on MSTIDs in solar maximum years is required to obtain detailed information of the climatology of MSTIDs during geomagnetic disturbances.

4.2. Nighttime MSTIDs

[33] While the nighttime and daytime MSTIDs are similar in period and propagation azimuth, they show significant difference in amplitude, propagation velocities and durations. Nighttime MSTIDs propagate at an average velocity ~40% slower than that of daytime ones. And the average duration of nighttime MSTIDs exceeds that of daytime ones by a factor of ~130%. The ranges of the period and velocity of nighttime MSTIDs in the present study (20–70 min and 50–230 m/s, respectively) are in agreement with other observations at similar magnetic latitudes (e.g., Japan and Puerto Rico [*Kotake et al.*, 2007; *Garcia et al.*, 2000]) and at slightly higher latitudes (e.g., California [*Tsugawa et al.*, 2007]). Slower MSTIDs, with a velocity range of 50–100 m/s, have been observed using an array of OI all-sky imagers in Japan [*Shiokawa et al.*, 2003]. This finding may indicate a height dependence of nighttime MSTIDs velocity, as the OI nightglow has an emission layer at a height of 200–300 km and GPS TEC includes disturbance information in the ionosphere above 300 km.

[34] There exist two important features of nighttime MSTIDs, as reported in previous studies and deduced from the present observations: they tend to propagate southwestward in the Northern Hemisphere, regardless of season or latitude; and their occurrence shows a peak in June, around the summer solstice. For nighttime MSTIDs, the maximum occurrence (50–60%) is found in June, for both our GPS network and nightglow observations [*Shiokawa et al.*, 2003]. The southwestward preference of nighttime MSTIDs is not consistent with the conventional wind-filtering theory, which predicts a northward direction of MSTIDs due to the filtering effect of the thermospheric wind blowing equatorward at night. The peak occurrence of nighttime MSTIDs around the summer solstice is different from the seasonal behavior of MSTIDs caused by AGWs from the lower atmosphere, which show a peak occurrence at the winter solstice, as stated above. In addition, the occurrence of nighttime MSTIDs shows a decrease with increasing Kp index (Figure 8). Hence, the cause of nighttime MSTIDs is related to phenomena other than meteorological processes and auroral activity.

[35] Many authors have proposed that F region electrodynamic forces such as Perkins instability play an important role in the generation of nighttime MSTIDs [*Perkins*, 1973; *Tsugawa et al.*, 2007; *Kelley and Miller*, 1997; *Kelley and Makela*, 2001; *Kelley et al.*, 2002]. Spatial variations in F region plasma density can generate local polarized electric fields, which are short-circuited by high conductivity in the E region during daytime but are maintained at night due to reduced conductivity [*Kotake et al.*, 2007]. The polarization electric field moves the plasma via $\mathbf{E} \times \mathbf{B}$ drift, giving rise to perturbations in plasma density. *Perkins* [1973] reported that the growth and damping of ionospheric plasma due to midlatitude electrodynamics are strongly dependent on azimuth. However, while most of nighttime MSTIDs propagate westward, Perkins theory predicts an eastward direction under average background conditions [*Kelley and Makela*, 2001]. Based on the observation of airglow and incoherent scatter radar at Arecibo, *Kelley and Makela* [2001] and *Kelley et al.* [2002] suggested that, besides the linear process proposed by *Perkins* [1973], nonlinear development of polarization electric fields should be involved in the formation of nighttime MSTIDs.

[36] The model of Perkins instability can explain the occurrence peak of nighttime MSTIDs at the summer solstice, because the growth rate of a Perkins instability is inversely proportional to the neutral density [*Perkins*, 1973; *Kotake et al.*, 2007], and the density in the thermosphere shows a minimum at the solstices [*Moore and Boulton*, 1987]. There occurs a major peak in the occurrence of nighttime MSTIDs at the June solstice and a slight increase in the occurrence in December, near the winter solstice (Figure 5). Our observations of the seasonal behavior of nighttime MSTIDs are in good agreement with the behavior predicted by the model of Perkins instability.

[37] Though previous observations revealed that some nighttime MSTIDs were related to AGWs from the lower atmosphere, such MSTIDs appear to be rare in the present statistical results. The sources of AGWs (e.g., the jet stream)

are active during both night and day. Previous observations by Doppler interferometer radar revealed upgoing nighttime MSTIDs in the ionospheric D and E regions, which may be associated with AGWs from the lower atmosphere [*Adams et al.*, 1988]. In the China region, nighttime MSTIDs with a northward direction have been frequently observed by an HF Doppler array [*Ning et al.*, 1995] and are considered to be of meteorological origin. In fact, Figures 7d–7f show that ~8% of the nighttime MSTIDs propagate northward. Taking into account winds that blow equatorward in the evening, the northward propagation of nighttime MSTIDs is not consistent with the predictions of the electrodynamics wave model proposed by *Kelley and Miller* [1997], but is consistent with the wind filtering theory of AGWs. However, from a statistical perspective, such northward MSTIDs are not usually recorded by our GPS network, possibly because the amplitudes of ionospheric disturbances in TEC series with an electrodynamic origin are significantly larger than those caused by AGW from below in the evening. Accordingly, disturbances of electrodynamic origin dominate the wavefield, and we can only obtain information on disturbances with an electrodynamic origin from the DTEC series.

5. Summary

[38] The 15-month climatology of medium-scale traveling ionospheric disturbances during a solar minimum period was constructed from observations by a dense GPS receiver array in and around China. The GPS array included 50 GPS stations, with 24 stations located in Hubei province (29°N–33°N, 108°E–116°E). A total of 793 MSTID events were identified, with peaks at 1500 LT and 0100 LT. The occurrence of MSTIDs decreased following an increase in geomagnetic activity. The seasonal behaviors and regional properties of nighttime and daytime MSTIDs were analyzed, yielding the following results.

[39] (1) 46% of the MSTIDs occurred in the daytime. Daytime MSTIDs were characterized by a major occurrence maximum around the winter solstice and an equatorward preference for the propagation direction. The period, phase velocity, azimuth, and amplitude of daytime MSTIDs were 20–60 min, 100–400 m/s, 130°–270°, and 0.8–1.5%, respectively. The occurrence of MSTIDs decreased following an increase in geomagnetic activity. These features have been reported by many authors based on measurements by GPS TEC, HF Doppler, airglow imager, and satellite-based interferometer in various regions worldwide. The consistent propagation features of MSTIDs observed by various measurement techniques indicate a close relation among MSTIDs observed at different heights. The propagation direction and the seasonal behavior of MSTID occurrence support the view that daytime MSTIDs are an ionospheric manifestation of atmospheric gravity waves from the lower atmosphere.

[40] Previous HF observation of day-time MSTIDs in Central China revealed a major peak of occurrence in winter with a southeastward preference and a minor peak in summer with a northeastward preference. The latter peak is not found through GPS measurements in the present study. It is possible that northeastward-propagating MSTIDs observed by HF Doppler may have been filtered out at greater heights due to poleward-blowing background winds in the daytime.

[41] (2) The period, phase velocity, azimuth, and amplitude of nighttime MSTIDs are 20–70 min, 50–230 m/s, 170°–300°, and 2–7%, respectively. These MSTIDs tended to propagate southwestward and show a peak occurrence at the summer solstice. This type of MSTIDs has been observed previously by a GPS network and airglow in various regions (e.g., Japan, Taiwan, Puerto Rico and the USA). A possible excitation mechanism of nighttime MSTIDs is electrodynamic processes caused by plasma instability in the F layer [*Perkins*, 1973]. However, as noted by *Kelley et al.* [2002], it is likely that nonlinear mechanism be involved to explain the southwestward preference [*Kelley et al.*, 2002].

[42] **Acknowledgments.** We are grateful to the Scripps Orbit and Permanent Array Center (SOPAC) and IGS for providing GPS network data. This work was supported by the National Natural Science Foundation of China (grants 40974089, 41131066, 40931056, and 40974094), the National Important Basic Research Project of China (2011CB811405), and the Scientific Research Project of IHR, CMA (grant 1007).

[43] Robert Lysak thanks the reviewers for their assistance in evaluating this paper.

References

Adams, G. W., J. W. Brosnahan, and T. D. Halderman (1988), Direct radar observations of TIDs in the D- and E-regions, *J. Atmos. Terr. Phys.*, *50*, 931–935.

Afraimovich, E. L., E. A. Kosogorov, O. S. Lesyuta, I. I. Ushakov, and A. F. Yakovets (2001), Geomagnetic control of the spectrum of travelling ionospheric disturbances based on data from a global GPS Network, *Ann. Geophys.*, *19*, 723–731, doi:10.5194/angeo-19-723-2001.

Ashkaliev, Y. F., et al. (2003), Comparison of travelling ionospheric disturbance measurements with thermosphere/ionosphere model results, *Ann. Geophys.*, *21*, 1031–1037, doi:10.5194/angeo-21-1031-2003.

Baker, D. M., and K. Davies (1969), F2 region acoustic waves from severe weather, *J. Atmos. Terr. Phys.*, *31*, 1345–1346, doi:10.1016/0021-9169(69)90118-4.

Beach, T. L., M. C. Kelley, and P. M. Kintner (1997), Total electron content variations due to nonclassical traveling ionospheric disturbances: Theory and Global Positioning System observations, *J. Geophy. Res.*, *102*, 7279–7292.

Bertin, F., J. Testud, L. Kersley, and P. R. Rees (1978), The meteorological jet stream as a source of medium scale gravity waves in the thermosphere: An experimental study, *J. Atmos. Terr. Phys.*, *40*, 1161–1183, doi:10.1016/0021-9169(78)90067-3.

Boška, J., and P. Šauli (2001), Observations of gravity waves of meteorological origin in the *F* region ionosphere, *Phys. Chem. Earth*, *26*, 425–428.

Bristow, W., and R. Greenwald (1996), Multiradar observations of medium-scale acoustic gravity waves using the Super Dual Auroral Radar Network, *J. Geophys. Res.*, *101*(A11), 24,499–24,511, doi:10.1029/96JA01494.

Buss, S., et al. (2004), Analysis of a jet stream induced gravity wave associated with an observed stratospheric ice cloud over Greenland, *Atmos. Chem. Phys.*, *4*, 1183–1200, doi:10.5194/acp-4-1183-2004.

Candido, C. M. N., A. A. Pimenta, J. A. Bittencourt, and F. Becker-Guedes (2008), Statistical analysis of the occurrence of medium-scale traveling ionospheric disturbances over Brazilian low latitudes using OI 630.0 nm emission all-sky images, *Geophys. Res. Lett.*, *35*, L17105, doi:10.1029/2008GL035043.

Candido, C. M. N., I. S. Batista, F. Becker-Guedes, M. A. Abdu, J. H. A. Sobral, and H. Takahashi (2011), Spread F occurrence over a southern anomaly crest location in Brazil during June solstice of solar minimum activity, *J. Geophys. Res.*, *116*, A06316, doi:10.1029/2010JA016374.

Cowling, D. H., H. D. Webb, and K. C. Yeh (1971), Group rays of internal gravity waves in a wind-stratified atmosphere, *J. Geophys. Res.*, *76*, 213–220, doi:10.1029/JA076i001p00213.

Ding, F., W. Wan, and H. Yuan (2003), The influence of background winds and attenuation on the propagation of atmospheric gravity waves,

J. Atmos. Sol. Terr. Phys., *65*, 857–869, doi:10.1016/S1364-6826(03)00090-7.

Evans, J. V., J. M. Holt, and R. H. Wand (1983), A differential-Doppler study of traveling ionospheric disturbances from Millstone Hill, *Radio Sci.*, *18*, 435–451, doi:10.1029/RS018i003p00435.

Garcia, F. J., M. C. Kelley, J. J. Makela, P. J. Sultane, X. Pi, and S. Musman (2000), Mesoscale structure of the midlatitude ionosphere during high geomagnetic activity: Airglow and GPS observations, *J. Geophys. Res.*, *105*, 18,417–18,427, doi:10.1029/1999JA000306.

Georges, T. M. (1968), HF Doppler studies of traveling ionospheric disturbances, *J. Atmos. Terr. Phys.*, *30*, 735–746, doi:10.1016/S0021-9169(68)80029-7.

He, L., and J. Ping (2008), Occurrence of medium-scale travelling ionospheric disturbances identified in the Tasman international geospace environment radar observations, *Adv. Space Res.*, *42*, 1276–1280, doi:10.1016/j.asr.2007.06.010.

Hines, C. O. (1960), Internal atmospheric gravity waves at ionospheric heights, *Can. J. Phys.*, *38*, 1441–1481, doi:10.1139/p60-150.

Hocke, K., and K. Schlegel (1996), A review of atmospheric gravity waves and traveling ionospheric disturbances: 1982–1995, *Ann. Geophys.*, *14*, 917–940.

Hunsucker, R. D. (1982), Atmospheric gravity waves generated in the High-latitude ionosphere: A review, *Rev. Geophys.*, *20*, 293–315, doi:10.1029/RG020i002p00293.

Ibrahim, C., F. Chane-Ming, C. Barthe, and Y. Kuleshov (2010), Diagnosis of tropical cyclone activity through gravity wave energy density in the southwest Indian Ocean, *Geophys. Res. Lett.*, *37*, L09807, doi:10.1029/2010GL042938.

Jacobson, A. R., R. C. Carlos, R. S. Massey, and G. Wu (1995), Observation of traveling ionospheric disturbances with a satellite-beacon radio interferometer: Seasonal and local time behavior, *J. Geophys. Res.*, *100*(A2), 1653–1665, doi:10.1029/94JA02663.

Kelley, M. C., and J. J. Makela (2001), Resolution of the discrepancy between experiment and theory of midlatitude *F* region structures, *Geophys. Res. Lett.*, *28*, 2589–2592, doi:10.1029/2000GL012777.

Kelley, M. C., and C. A. Miller (1997), The electrodynamics of midlatitude spread F: 3. Electrobuoyancy waves? A new look at the role of electric fields and thermospheric gravity waves, *J. Geophys. Res.*, *102*(A6), 11,539–11,547.

Kelley, M. C., J. J. Makela, and A. Saito (2002), The mid-latitude F region at the mesoscale: Some progress at last, *J. Atmos. Sol. Terr. Phys.*, *64*, 1525–1529, doi:10.1016/S1364-6826(02)00090-1.

Kotake, N., Y. Otsuka, T. Tsugawa, T. Ogawa, and A. Saito (2006), Climatological study of GPS total electron content variations caused by medium-scale traveling ionospheric disturbances, *J. Geophys. Res.*, *111*, A04306, doi:10.1029/2005JA011418.

Kotake, N., et al. (2007), Statistical study of medium-scale traveling ionospheric disturbances observed with the GPS networks in Southern California, *Earth Planets Space*, *59*, 95–102.

Lee, C. C., Y. A. Liou, Y. Otsuka, F. D. Chu, T. K. Yeh, K. Hoshinoo, and K. Matunaga (2008), Nighttime medium-scale traveling ionospheric disturbances detected by network GPS receivers in Taiwan, *J. Geophys. Res.*, *113*, A12316, doi:10.1029/2008JA013250.

MacDougall, J. W., and G. E. Hall (1998), An F region height change produced by gravity waves, *Radio Sci.*, *33*(6), 1867–1876, doi:10.1029/98RS01787.

Martinis, C., J. Baumgardner, J. Wroten, and M. Mendillo (2010), Seasonal dependence of MSTIDs obtained from 630.0 nm airglow imaging at Arecibo, *Geophys. Res. Lett.*, *37*, L11103, doi:10.1029/2010GL043569.

Moore, P., and W. J. Boulton (1987), Some aspects of a global thermospheric density model deduced from the analysis of the orbit of intercosmos 13 rocket (1975–22b), *Planet. Space Sci.*, *35*(8), 1039–1052, doi:10.1016/0032-0633(87)90008-0.

Morton, F. W., and E. A. Essex (1978), Gravity wave observations at a southern hemisphere mid-latitude station using the total electron content technique, *J. Atmos. Terr. Phys.*, *40*, 1113–1122, doi:10.1016/0021-9169(78)90059-4.

Ning, B. Q., L. Li, and J. Li (1995), Variation of medium-scale traveling ionospheric disturbances at Wuhan, *Chin. J. Geophys.*, *38*(4), 439–447.

Perkins, F. (1973), Spread F and ionospheric currents, *J. Geophys. Res.*, *78*, 218–226, doi:10.1029/JA078i001p00218.

Pierce, A. D., and S. C. Coroniti (1966), A mechanism for the generation of acoustic gravity waves during thunderstorm formation, *Nature*, *210*, 1209–1210, doi:10.1038/2101209a0.

Pinger, W. H. (1979), Detection of traveling ionospheric disturbances with auroral zone incoherent scatter radar, *Radio Sci.*, *14*(1), 75–84, doi:10.1029/RS014i001p00075.

Richmond, A. D. (1978), Gravity wave generation, propagation, and dissipation in the thermosphere, *J. Geophys. Res.*, *83*, 4131–4145, doi:10.1029/JA083iA09p04131.

Saito, A., S. Fukao, and S. Miyazaki (1998), High resolution mapping of TEC perturbations with the GSI GPS network over Japan, *Geophys. Res. Lett.*, *25*, 3079–3082, doi:10.1029/98GL52361.

Seker, I., S. F. Fung, and J. D. Mathews (2011), Relation between magnetospheric state parameters and the occurrence of plasma depletion events in the nighttime midlatitude F region, *J. Geophys. Res.*, *116*, A04323, doi:10.1029/2010JA015521.

She, C. Y., and R. P. Lowe (1998), Seasonal temperature variations in the mesopause region at mid-latitude: Comparison of lidar and hydroxyl rotational temperatures using WINDII/UARS OH Height profiles, *J. Atmos. Sol. Terr. Phys.*, *60*, 1573–1583, doi:10.1016/S1364-6826(98)00082-0.

Shiokawa, K., C. Ihara, Y. Otsuka, and T. Ogawa (2003), Statistical study of nighttime medium-scale traveling ionospheric disturbances using mid-latitude airglow images, *J. Geophys. Res.*, *108*(A1), 1052, doi:10.1029/2002JA009491.

Tsugawa, T., Y. Otsuka, A. J. Coster, and A. Saito (2007), Medium-scale traveling ionospheric disturbances detected with dense and wide TEC maps over USA, *Geophys. Res. Lett.*, *34*, L22101, doi:10.1029/2007GL031663.

Tsutsui, M., and T. Ogawa (1973), HF Doppler observation of ionospheric effects due to typhoons, *Rep. Ionos. Space Res. Jpn.*, *27*, 121–123.

Waldock, J. A., and T. B. Jones (1984), The effects of neutral winds on the propagation of medium scale atmospheric gravity waves at mid-latitudes, *J. Atmos. Terr. Phys.*, *46*, 217–231, doi:10.1016/0021-9169(84)90149-1.

Waldock, J. A., and T. B. Jones (1986), HF Doppler observations of medium-scale travelling ionospheric disturbances at mid-latitudes, *J. Atmos. Terr. Phys.*, *48*, 245–260, doi:10.1016/0021-9169(86)90099-1.

Wan, W. X., B. Q. Ning, H. Yuan, J. N. Li, L. Li, and J. Liang (1997), TID observation using a short baseline network of GPS receivers, *Acta Geodyn. Geophys. Hung.*, *32*(3–4), 321–327.

Wan, W. X., H. Yuan, B. Ning, and J. Liang (1998), Travelling ionosphere disturbances associated with tropospheric vortexes around Qinghai-Tibet Plateau, *Geophys. Res. Lett.*, *25*, 3775–3778, doi:10.1029/1998GL900030.

Wan, W. X., H. Yuan, B. Ning, and J. Liang (2000), Regional properties of travelling ionospheric disturbances observed in central China, *Adv. Space Sci.*, *25*, 219–222.

Wang, M., et al. (2007), Monitoring global traveling ionospheric disturbances using the worldwide GPS network during the October 2003 storms, *Earth Planets Space*, *59*, 1–13.

Xiao, Z., S. Xiao, Y. Hao, and D. Zhang (2007), Morphological features of ionospheric response to typhoon, *J. Geophys. Res.*, *112*, A04304, doi:10.1029/2006JA011671.

Yokoyama, T., Y. Otsuka, T. Ogawa, M. Yamamoto, and D. L. Hysell (2008), First three-dimensional simulation of the Perkins instability in the nighttime midlatitude ionosphere, *Geophys. Res. Lett.*, *35*, L03101, doi:10.1029/2007GL032496.

Zhou, Q., and J. D. Mathews (2006), On the physical explanation of the Perkins instability, *J. Geophys. Res.*, *111*, A12309, doi:10.1029/2006JA011696.

F. Ding and W. Wan, Beijing National Observatory of Space Environment, Institute of Geology and Geophysics, Chinese Academy of Sciences, Beijing 100029, China. (dingf@mail.iggcas.ac.cn)

J. Wang, G. Yang, and T. Yu, National Center for Space Weather, China Meteorological Administration, Beijing 100081, China.

G. Xu, Institute of Heavy Rain, China Meteorological Administration, No. 3 Rd Donghudonglu, Hongshan District, Wuhan 430074, China.